PAPER

Wetting and spreading of liquid lithium onto nanocolumnar tungsten coatings tailored through the topography of stainless steel substrates

IOP Publishing | International Atomic Energy Agency Nuclear Fusion

Nucl. Fusion **60** (2020) 126033 (11pp) https://doi.org/10.1088/1741-4326/abb53e

Wetting and spreading of liquid lithium onto nanocolumnar tungsten coatings tailored through the topography of stainless steel substrates

S. Muñoz-Piña[1,2], A. Garcia-Valenzuela[3], E. Oyarzabal[4], J. Gil-Rostra[3], V. Rico[3], G. Alcalá[2], R. Alvarez[3,5], F.L. Tabares[4], A. Palmero[3] and A.R. Gonzalez-Elipe[3]

[1] Nano4Energy SLNE, c/Jose Gutiérrez Abascal 2, 28006 Madrid, Spain
[2] Universidad Complutense de Madrid, Facultad de Ciencias Químicas, Dep. Ingeniería Química y de Materiales, Av Complutense s/n, 28040 Madrid, Spain
[3] Instituto de Ciencia de Materiales de Sevilla (CSIC-US), Américo Vespucio 49, 41092 Seville, Spain
[4] CIEMAT, Fusion Department, Av Complutense 40, 28040 Madrid, Spain
[5] Departamento de Física Aplicada I, Escuela Politécnica Superior, Universidad de Sevilla, c/Virgen de África 7, 41011 Seville, Spain

E-mail: alberto.palmero@csic.es and paco.tabares@ciemat.es

Received 13 July 2020, revised 31 August 2020
Accepted for publication 4 September 2020
Published 21 October 2020

Abstract

The use of liquid metal as an alternative to cover the plasma-exposed areas of fusion reactors has called for the development of substrates where refilling and metal spreading occur readily and at reasonably low temperatures. In the search for common materials for this purpose, we show that nanostructured tungsten coatings deposited on stainless steel (SS) by magnetron sputtering at oblique angles (MS-OAD) is a good option, provided that the surface microstructure of substrate is properly engineered. Tungsten thin films with nominal thicknesses of 500 and 2500 nm were deposited onto SS plates subjected to conventional surface finishing treatments (sand blasting, sand paper abrasion and electrochemical polishing) to modify the surface topography and induce the appearance of different groove patterns. In the first part of this work we show how the topographical features of the SS substrates affect the typical nanocolumnar microstructure of OAD thin films of tungsten. Subsequently, we characterize the spreading behavior of liquid lithium onto these tungsten nanocolumnar surfaces and critically discuss whether nanocolumnar tungsten thin films are a suitable option for the wetting and spreading of molten lithium. As a result, we reveal that the features of the tungsten nanocolumnar coating, characterized by a given height and void spaces between nanocolumns in the order of 1–2 μm, is critical for the spreading of molten lithium, while the existence of wider channels affects it very weakly. Moreover, it is shown that tungsten films deposited by MS-OAD on SS substrates subjected to conventional finishing procedures represent a good alternative to other more complex surface engineering procedures utilized for this purpose.

Supplementary material for this article is available online

Keywords: tungsten films, OAD, MS, liquid lithium, CPS, PFC, divertor targets, wetting, spreading

(Some figures may appear in colour only in the online journal)

1. Introduction

The selection of suitable plasma facing components (PFC) for future fusion reactors, able to withstand power densities up to 20 MW m^{-2} in a cyclic operation, is a challenge that is pushing the development of a large variety of innovative solutions [1]. Although solid tungsten is the base line option for operational power densities up to 10 MW m^{-2} as those expected in ITER [2], the higher powers foreseen for other reactors, together with the need of withstand strong neutron irradiation and high temperatures, have motivated the search for alternative materials and magnetic configurations. Among the firsts, liquid metals (LMs) have emerged as a mature and suitable alternative because, contrary to solid materials, they avoid a permanent damage of walls and offer refilling and substitution capacities that are critical for this application. Lithium, tin and their alloys are being considered as suitable LMs at present [3]. In this way, and even though free flowing concepts have been proposed to enable continuous particle and power exhaust operation [4], static designs, based on the use of capillary forces to hold the LM onto the reactor walls, are the preferred options in current proposals. One of the available designs is the so-called capillary porous system (CPS) [5], in which a liquid metal pool is put into contact with a porous metallic mesh through which the LM can flow. Typical pore sizes are in the range of few microns and, although smaller pore radii would involve higher capillary holding forces, other undesired phenomena, such as viscosity-associated effects that hinder the refilling of the surface exposed to the plasma [6] as well as other material-related compatibility issues such as corrosion, embrittlement or hydrogen solubility limit the design and final choice of materials.

In the quest for the most adequate solution, there is an intense search to find optimal geometries and topographies for CPS. Molten lithium capillary pumping can be integrated into the PFC by adapting the surface to promote wicking. Sintered porous materials, wire meshes, and other direct metal vapor deposition methods have been shown to be capable of passively wicking molten lithium [7]. However, neither sintered porous materials nor wire meshes can be easily integrated into a structural material in a plasma environment. A method to produce a structure capable of promoting the wicking of liquid metals, is to machine narrow channels with widths on the scale of tens of microns into the surface of the PFC. Laser micro machining is one of the means employed to produce these features with minimal impact on the underlying high temperature and structural material properties [8, 9].

In this work, we investigate the possibility of using nanostructured tungsten coatings deposited on conventional stainless steel (SS) substrates as efficient spreading surfaces of LMs. The main concept sustaining this proposal is the fabrication of nanostructured surfaces of tungsten where a LM may effectively diffuse thanks to superficial capillary forces acting as in the CPS approach [5]. This combination of a SS substrate and a tungsten coating offers the synergetic advantage of combining a relatively cheap and easily malleable substrate material (SS) with a tungsten coating of proved chemical resistance to LMs. Although the poor thermal conductivity of SS precludes its use in high heat flux components of fusion reactors, the technology developed here can be easily extended to more relevant substrate materials, such as tungsten and its alloys. In particular, for the manufacturing of the investigated W/SS layered system, we have subjected the SS substrates to conventional abrasion and finishing procedures to modify their roughness and surface topography and to design certain patterns onto their surface. Then, tungsten thin films of approximately 500 and 2500 nm of thickness were deposited onto these substrates by magnetron sputtering in an oblique angle configuration (MS-OAD), well-known for promoting the growth of nanocolumnar and highly porous layer structures [10]. This configuration relies on the oblique incidence of gaseous deposition species on a substrate that, thanks to so-called surface shadowing mechanisms, initiate a self-organization phenomenon that end up with the formation of tilted nanocolumnar structures. While these layers have been classically grown by the evaporation technique [11], MS-OAD has emerged in the last years as a versatile and reliable approach [12]: in this case, gaseous deposition species are produced by the interaction between a plasma and a solid target in a vacuum reactor [13] and are subsequently deposited on a substrate [14]. Most common strategies to achieve the oblique incidence of sputtered species rely on tilting the substrate holder with respect to the target [15], although there are other geometrical approaches [16].

Porous nanocolumnar coatings grown in an oblique angle configuration have been deeply studied for numerous applications [17–20]: these are formed by a vast array of tilted nanocolumnar structures with diameters in the order of few tens nm and a typical center-to-center distance from few hundred nm to few microns [21], conforming a well-connected open and embedded nano/micro channel network [22]. On conventional flat substrates, these nanocolumnar structures distribute homogeneously over the surface and define a rough surface topography with typical sizes below those of common CPS surfaces. Yet, despite its obvious importance, little is known about the influence of the roughness or topographic patterns on the substrate on the nanostructure of OAD films [23–26], which is known to affect the nano/micro channel network: in a previous publication, we demonstrated that when the substrate contains large topographic patterns, the nanocolumnar arrangement tend to enhance these patterns, up to a critical film thickness, the so-called *Oblivion Thickness*, with typical values in the order of few microns [16], above which the columnar arrangement tends to randomize and spread homogeneously over the substrate, likewise on a flat surface. This result opens up the possibility to tailor the features of the film nanocolumnar network, i.e. void size distribution and connectivity, by using wisely chosen patterned substrates, as long as the film thickness is kept low enough. The main aim of the present work is to develop a surface that, preserving the typical features of MS-OAD thin films, may reproduce a CPS effect through

the deposition of nanocolumnar tungsten onto SS patterned surfaces.

Herein, we empirically apply these concepts to the MS-OAD of tungsten thin films on previously abraded and/or patterned SS substrates and characterize the evolution of surface topography of the studied W/SS systems as resulting from an interplay between deposition geometry and influence of substrate roughness/pattern. This analysis has provided clear guidelines for the fabrication of surface nanostructures capable of reproducing the function of a CPS spreading layer. Lithium wetting and spreading tests carried out onto different W/SS specimen showed a better spreading of LM onto W/SS surfaces where deposited tungsten preserves the nanocolumnar topography found on ideal flat substrates or where film nanocolumns arranged along 1D large grooves previously carved on the SS substrates. The topographic characteristics of some of these W/SS surfaces are critically discussed in relation to their capacity to favor the spreading of a LM.

2. Experimental

2.1. Stainless steel substrates

SS substrates of 2×2 cm^2 (grade 304) were used for the different experiments. Si (100) substrates of 1×1 cm^2 were used for specific characterization of the deposition of W thin films on a flat substrate. SS substrates were polished by different methods as summarized in table 1 and labeled as indicated there. Substrates #1 and #2 correspond to a flat silicon wafer piece and to a pristine SS foil. Substrates #3 were obtained by sandblasting #2 type substrates in a perpendicular arrangement to the sand flux for 1 min. A standard sandblasting machine was employed for this purpose (Chorreadora, model: mega and system seco made by Abrasivos y Maquinaria S.A.). Substrates #4 were obtained by means of a Struers Labopool 5 automatic polishing machine using different abrasive grade sandpapers. In this way, #2 type substrates were kept at a fixed position in contact with a rotating plate of ca. 50 cm diameter at a speed of 200 rpm. The abrasive grade of the sandpaper was changed after each minute of treatment following this sequence: P240 (abrasive particle diameter 55 μm), P400 (abrasive particle diameter 35 μm), P600 (abrasive particle diameter 25 μm) and P800 (abrasive particle diameter 20 μm). Substrates type #5 were obtained by continuing the sequence employed for substrates #4 with a P1200 (abrasive particle diameter 16 μm) and a P2500 (abrasive particle diameter 5 μm) grade sandpaper. Substrates #6 were obtained by taking substrates type #5 and continuing the polishing process with a Struers DP-Spray ~ 3 μm and a ~ 1 μm polycrystalline diamond particles sprayed cloth for $1 + 1$ min. Finally, substrates #7 were obtained by applying an electrochemical polishing method on substrates #6: half part of substrate #6 was covered with a Kapton tape for protection and the piece was submerged into a solution of H_3PO_4:H_2SO_4 (42 ml H_3PO_4 and 28 ml H_2SO_4). Electropolishing was carried out by applying a constant current of 1 A with an ISO-TECH power supply IPS1603D for 300 s [27]. In this way, half substrate is type #6 and the other half type #7.

2.2. Characterization procedures

Confocal microscopy analysis was carried out with a ZEISS LSM 7 DUO microscope in the CITIUS of the University of Seville. Surface roughness of the samples was obtained from the confocal surface images by calculating the quadratic dispersion of the surface heights. Reflectivity spectra were recorded at 30º incident angle using a Cary 100 instrument. Field emission scanning electron microscopy (FESEM) images were recorded using a Hitachi S4800 microscope at the Instituto de Ciencia de Materiales de Sevilla (CSIC-US, Seville, Spain). Film thickness was checked in all the cases by analyzing cross-sectional FESEM images of the films grown on Si (substrate #1).

2.3. Deposition and characterization of nanocolumnar tungsten thin films

All substrates #1–#7 were coated following the same procedure. W films were grown using the magnetron sputtering setup described in reference [17]: a 7.5 cm diameter W target was used, while the substrate holder was grounded and located 7 cm apart, maintaining an argon pressure in the reactor of 0.2 *Pa*. Moreover, it was turned an angle of 100º with respect to the target surface to ensure that the W atoms steaming from the racetrack (radius $\sim$2.5 cm) arrived at the substrate along an average angular direction of 85º with respect to the substrate normal [28]. Films were grown on substrates #1–#7 in two different runs. The targeted film thickness was 500 and 2500 nm, respectively (deposition time of 80 and 400 min, respectively), that were corroborated by the cross-sectional FESEM images of the films deposited on substrate #1. Samples will be designated in the text according to: *W/#substrate-thickness*, where *thickness* refers to the equivalent thickness of W determined on a flat substrate during the same deposition experiment, for example, sample W/#5-2500 refers to a sample consisting of a thickness of 2500 nm of tungsten deposited on substrate #5.

The FESEM images of the nanocolumnar film were analyzed by means of a home-made image analysis software (IDUN, Image Domains Uncovered) that analyzed the columnar arrangement and coalescence, already employed in ref [29]. The software IDUN identifies all well-connected regions in a given image, and operates following the sequential protocol: (i) the brightness and contrast of the image are locally enhanced to avoid inhomogeneities; (ii) the image is converted into a black and white binary map; (iii) features with size below certain threshold are considered noise and are removed and (iv) a MatLAB-based numerical routine is employed to differentiate each independent domain (two columns are considered to belong to the same domain if there is a continuum path from one to the other). A version of this software, incorporating a user-friendly interface, can be freely downloaded from our webpage [30]. For more details on the IDUN software, please check the user manual.

Table 1. List of substrates and polishing technique employed for their surface finishing. Last column indicates the surface roughness[a] of each substrate as obtained by confocal microscopy.

	Polishing	Features	Roughness
#1	No	Silicon (100) Substrate.	<1 nm
#2	No	Original stainless steel substrate.	350 nm
#3	Sandblast	Standard treatment.	1350 nm
#4	Sandpaper	Struers Labopol 5 automatic polishing machine. Sandpaper with final abrasive grade of P800.	120 nm
#5	Sandpaper	Struers Labopol 5 automatic polishing machine. Sandpaper with final abrasive grading of P2500.	70 nm
#6	Polishing cloth	Final treatment with ~ 1 μm polycrystalline diamond particles sprayed cloth	50 nm
#7	Electrochemical Methods	Standard H_3PO_4:H_2SO_4-based method.	35 nm

[a]Roughness defined as the quadratic dispersion of surface heights.

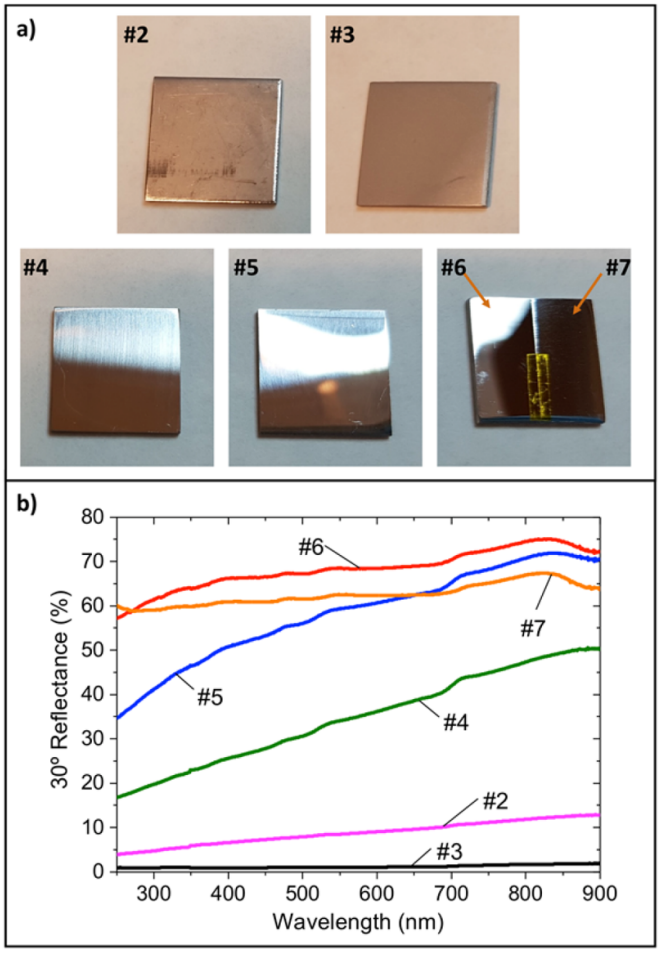

Figure 1. (Top) Series of photographs of substrates #2–#6/7. (Bottom) Reflectance spectra of substrates #2–#6/7.

2.4. Li wetting experiments

To prove the LM spreading performance of W/SS systems, several experiments have been performed at the Plasma Wall Interaction Laboratory (CIEMAT). The set up consists of a stainless steel vacuum chamber with an oven filled with lithium that can be heated up to 600 °C with a resistance heater. It also has a sample manipulator that allows for the free movement of samples inside the chamber. On the upper part of the oven, a window with a shutter to avoid lithium deposition/condensation on the glass provides direct visual inspection of the state of the samples during the experiments. The wetting temperature of the samples is achieved by manually dipping the sample in successive LMs at increasing temperatures. Tests started at 250 °C–300 °C, and the sample was inserted in the LM at 10 °C intervals for 10 s (the time that samples need to thermally equilibrate with the liquid lithium) and then extracted to visually observe if the specimen wetted or not.

Once reached the wetting temperature, the oven is further heated up to around 400 °C–420 °C to follow the evolution of the wetted area of the samples. An image of the specimen is obtained for each temperature to record the changes. Two relevant temperatures were taken into consideration for each sample, the temperature at which initial wetting is observed (T_w), and the temperature at which the Li starts to spread out above the zone inserted in the liquid (T_s). Results for a typical experiment are reported as **supplementary material**, where figure S1 (available online at https://stacks.iop.org/NF/60/126033/mmedia) shows as example a series of images taken for specimen W/#5-2500 after immersion in the LM at 10 °C intervals from 350 °C to 380 °C. It is apparent in these images that the LM initially wets the surface and then progressively spread onto the specimen surface. From this set of images, we can define a Tw of 360 °C and a Ts of 380 °C for this particular sample. For specimen with a directional surface pattern (see results section), wetting experiments were performed along a vertical and a horizontal orientation of the grooves with respect to the LM surface in order to observe a possible effect of orientation in the wetting and spreading of the LM. All these measurements were taken with a chamber pressure in the range (1.3–6.6) $\times$ 10^{-4} Pa

3. Results and discussion

3.1. Surface morphology of SS substrates

Figure 1 shows a basic characterization of the different SS substrates (#2–#7) employed for the experiments. In figure 1(*a*), showing the optical images of the substrates, it is apparent that the polishing method directly affects the reflection of light and transforms the specimen aspect from mate to mirror-like. The measured reflectivity spectra of the substrates at an angle of 30º are shown in figure 1(*b*), where we can notice that the original (#2) and sandblasted (#3) substrates have reflectivity values lower than 15% and 5% respectively in the whole studied spectral range, whereas higher reflectivity values are found for

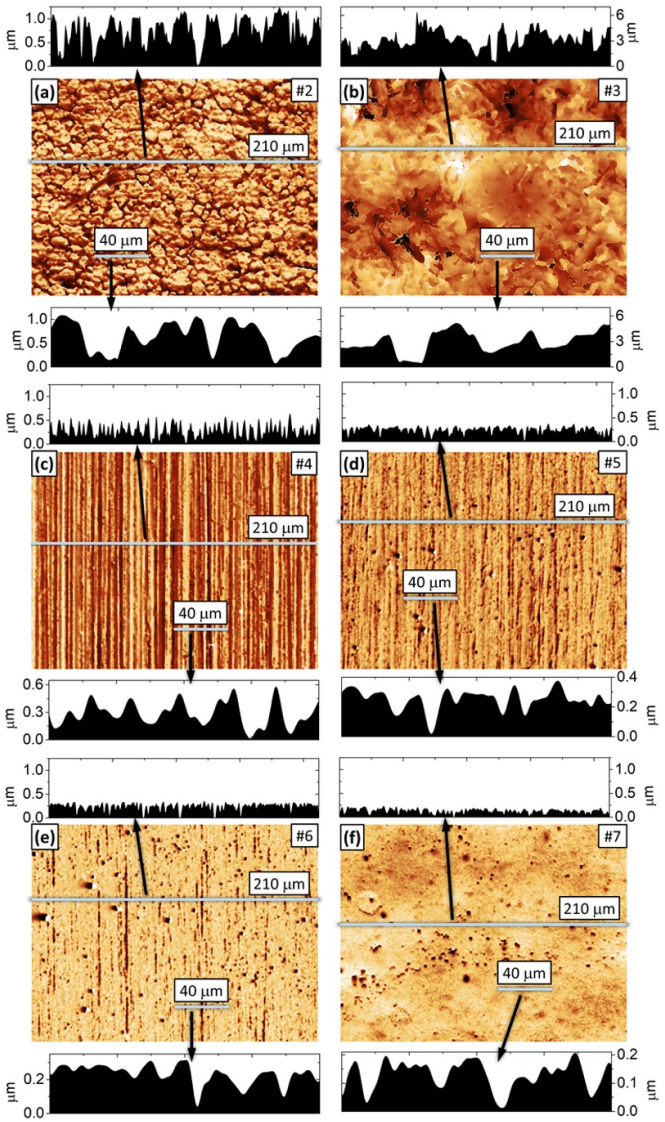

Figure 2. Optical confocal microscopy images and linear topographic profiles taken along the lines marked in the micrographs (two different profiles, of lengths 210 μm and 40 μm, for each one) for substrates #2–#6/7 as indicated. The linear profiles clearly visualize the lateral and in-depth dimensions of the grooves and topographic features existing in the substrates. For comparison purposes, the 210 μm long profiles all have the same Y scale (except for the roughest one, at (*b*), with a magnification 6 times lower). For the 40 μm long profiles the Y scale has been chosen to maximize the detail level. The magnification factors relative to the 40 μm profile in (*a*) are: 0.17 for (*b*); 2.00 for (*c*); 2.86 for (*d*); 3.33 for (*e*), and 6.67 for (*f*).

substrates #4, #5, #6 and #7. The different reflectivity of SS substrates is a result of their different surface features/roughness, as determined by confocal microscopy (see the confocal images and lineal roughness profiles in figure 2 and the measured roughness parameters in table 1). From these morphological characterization data it appears that the original substrate #2 (figure 2(*a*)) possesses a granular surface with a typical grain diameter of few microns, which determines a relatively high roughness value of $\sim$ 350 nm. The fact that this original substrate is not polished and contains numerous imperfections and damaged areas, explain its low reflectivity and high roughness. The surface of the sandblasted substrate #3 in figure 2(*b*) presents an even greater damage and the appearance of large irregular structures that render a value of surface roughness of about $\sim$ 1350 nm, i.e. 3–4 times higher than that of the original substrate. This causes the light to be highly dispersed, with a reflectance below 5% (figure 1(*b*)). Interestingly, the surface features in substrate #3 were approximately three times higher and two-three times wider than in sample #2 (see linear profiles in figure 2). Substrate #4 was obtained after sequentially polishing substrate #2 with different abrasive sandpapers with small particle size. Its topographic image and linear profiles (depicted in figure 2(*c*)) show the presence of well-defined and regular linear grooves with heights ranging between 0.3–0.5 μm that are separated by about 6–7 μm. The calculated surface roughness of this substrate was 120 nm. This value, lower than that of the original substrate (#2) and much lower than that of the sandblasted one (#3), accounts for a reflectivity up to 50% at long wavelengths, substantially higher than that of the previous two cases. Moreover, substrate #5, which underwent a similar finishing procedure but using an additional abrasive sandpaper treatment with particle sizes down to 5 μm, depicts a similar topography (see figure 2(*d*)) where the grooves separated by a similar 6–7 μm width have now a smaller height between 0.1–0.3 μm. The calculated surface roughness of this substrate is 70 nm and its reflectivity varies from 35% (for wavelengths of $\sim$ 200 nm) up to 70% (for wavelengths of $\sim$ 900 nm) (see figure 1(*b*)). Substrate #6 in figure 2(*e*), obtained from #5 after polishing with diamond nanoparticles with sizes down to 1 μm and a polishing cloth, shows some traces of the grooves existing in #5, but the surface roughness has been reduced down to $\sim$50 nm and the height of surface features to 0.1–0.2 μm, yielding a higher reflectance around 70% for wavelengths between 200 and 900 nm (see figure 1(*b*)). Finally, substrate #7, obtained applying an additional electrochemical polishing procedure, depicts a surface with no apparent patterns and a minimum surface roughness of $\sim$ 35 nm (see figure 2(*f*)), feature height less than 0.1–0.2 μm and a reflectance profile around 60% in whole spectral range under study (figure 1(*b*)).

3.2. Growth of nanocolumnar OAD W thin films on rough and patterned substrates

To understand the growth of the nanocolumnar OAD tungsten films on the rough and patterned SS substrates, we firstly analyzed the deposition process on a flat surface (substrate #1). Figure 3 shows the top-view and cross-section FESEM micrographs of an OAD W thin film of 2500 nm thickness grown on a Si substrate. The microstructure of this thin film is made up of large tilted isolated nanocolumns and bundles of nanocolumns of approximately 2 μm height and separated by void spaces with typical lengths varying between 1 and 3 μm. The nanocolumns are asymmetric in cross section and have an average width below 1 μm at the tip head. Their average surface density is roughly 180 nanocolumns per 400 μm^2. Interestingly, these nanocolumns develop from a first layer denser in smaller and thinner nanocolumns (see micrographs

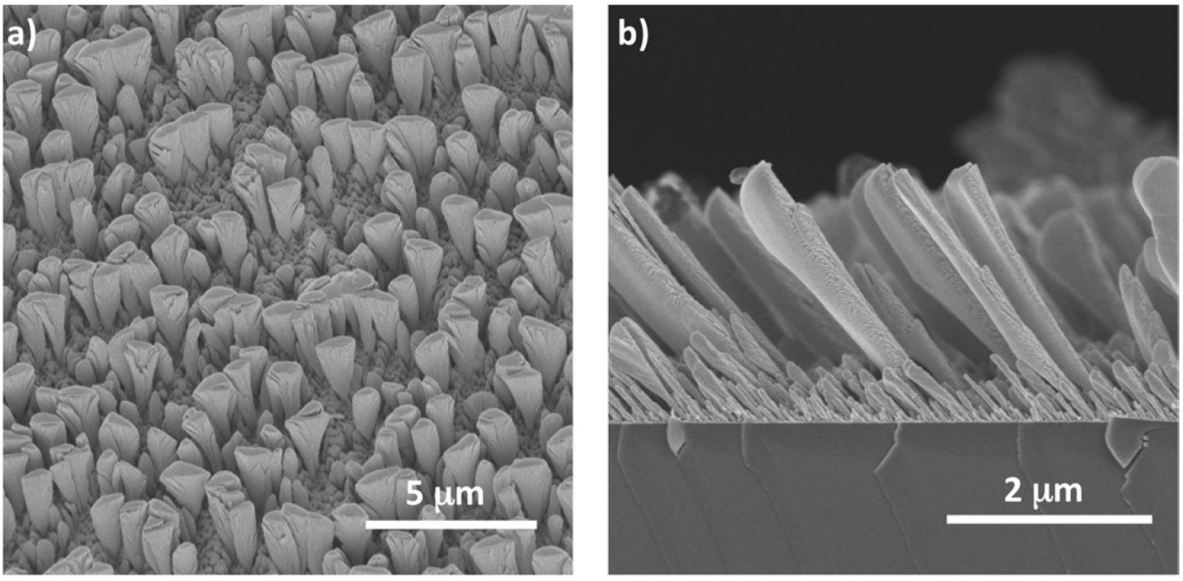

Figure 3. (*a*) Top view and (*b*) cross section FESEM micrographs of a tungsten thin film of 2500 nm thickness deposited onto a silicon substrate.

in figures 3(*a*)–(*b*)) with lengths of around 500 nm. A growth process characterized by the self-organization of the initially formed small nanocolumns is a typical feature of OAD thin films, which is exalted for the tungsten films prepared in the present work where deposition has been carried out at a very high glancing angle (see experimental section). This evolution can be understood as the result of a competitive growth of nanocolumns mediated by surface shadowing mechanisms [10–12, 16].

The nanostructuration mechanism of OAD thin films is modified when performing the deposition on treated SS substrates characterized by different surface topographies. The evolution in surface microstructure follows the general principles of the deposition of OAD thin films on rough substrates [16]. Figure 4 shows the FESEM images of the different W/#SS specimens prepared in the present work for the two equivalent thicknesses of tungsten described in section 2.3. In this set of images, it is apparent that in specimens W/#SS-500 the big surface features characterizing the different #SS substrates remain almost unaltered, though small features due to the little nanocolumns typical of the 500 nm tungsten thin films superimpose on the original topography (see figure 3). According to the available knowledge about the growth of OAD thin films on rough substrates, this situation is typical of the *substrate-driven growth stage* appearing for thin OAD thin films with a thickness smaller than the *oblivion thickness* [16].

The situation drastically changes for tungsten thin films of 2500 nm equivalent thickness. In this case, well-defined nanocolumns, similar to those found on the flat silicon substrate (see figure 3), are produced on all #SS substrates but #3. The absence of well-defined tungsten nanocolumns in sample #3/W-2500 indicates that the large surface protrusions existing in the SS sand-blasted substrate preclude the shadow mechanisms responsible for the formation of nanocolumns [16, 31, 32]. This can be explained assuming that the big surface features at the substrate surface induces a broad distribution of local incidence angles for the sputtered W atoms, inhibiting the formation of nanocolumns over its surface (this basic tendency does not contradict the appearance, confined to small areas, of small nanocolumns in specimen #3/W-500 nm). In samples W/#6-2500 and W/#7-2500, where the SS substrate is characterized by a much smaller roughness, large and well-defined tungsten nanocolumns appear randomly distributed onto the surface. In specimens W/#4-2500 and W/#5-2500, similar nanocolumns arrange along the grooves featuring the surface of these SS substrates. Regarding the growth process mechanisms, the formation of tungsten nanocolumns in specimen W/#2,/#4,/#5,/#6,/#7-2500 correspond to a growth defined by substrate features [16]. In the same line, micrographs in figures 4(*i*) and (*l*) also suggest that the equivalent thickness of 2500 nm is closer to the *Oblivion Thickness* for substrates #4 and #5, although the specific features of the substrate topography still remain noticeable after the deposition of these thicker films.

3.3. LM wetting and spreading on W/#SS

The tailored growth of different thin film morphologies mediated by the topography of SS substrates provided a variety of tungsten surfaces with different responses towards LM wetting and spreading. Figure 5 shows the evolution of the two critical temperatures (T_w and T_s) for the studied #SS substrates and W/#SS specimen. It is apparent in figure 5(*a*) that T_w for specimen W/#SS-500 and W/#SS-2500 only varied within the short interval comprised between 330 °C and 360 °C, while larger variations occurred for the bare #SS substrates, where T_w decreased following the same tendency that the roughness (see table 1), from 360 °C (sample #2) to 270 °C (samples #6/7). These evidences sustain that for flat specimens wetting

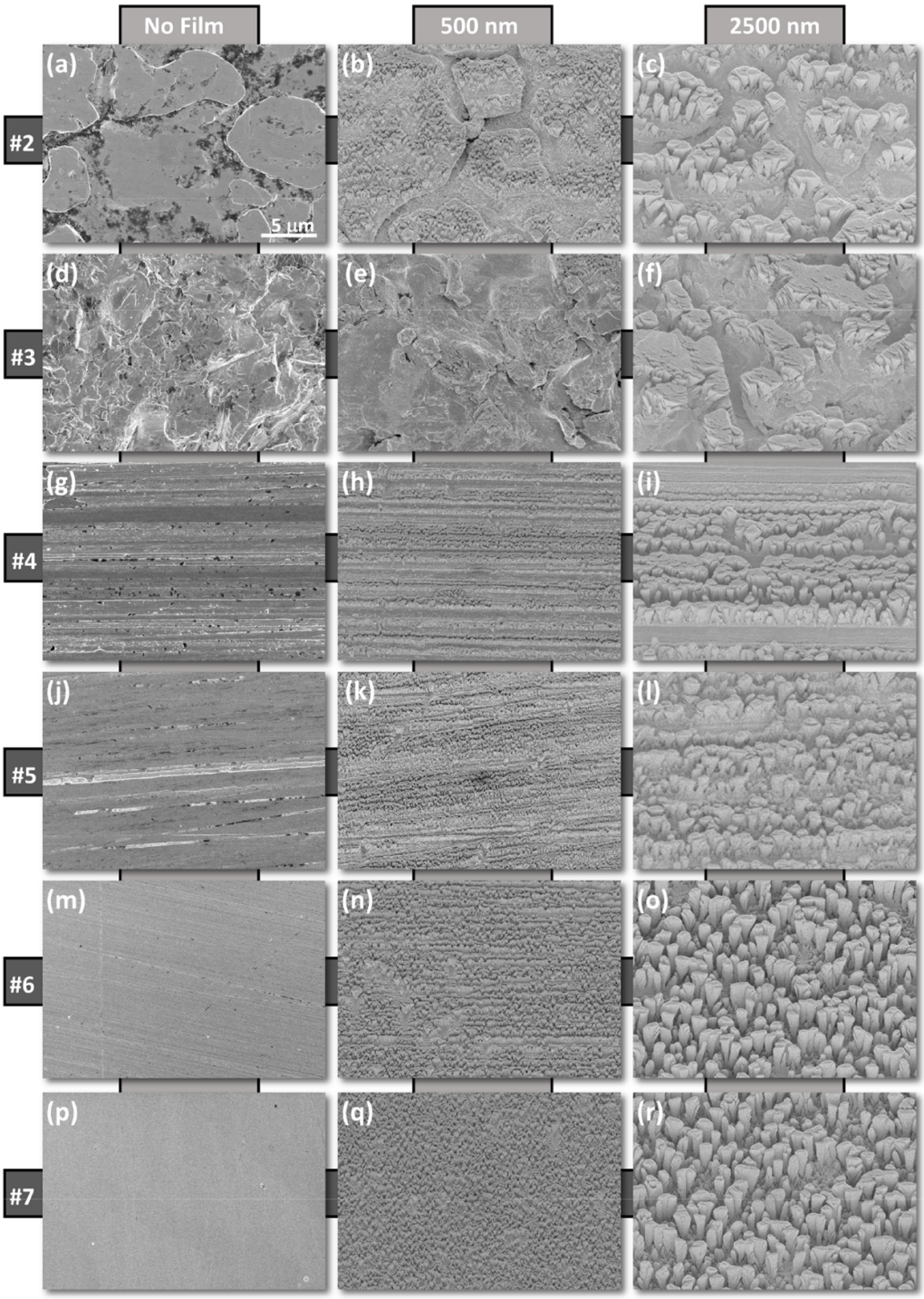

Figure 4. SEM top view micrographs of #SS substrates and specimen W/#SS-500 and W/#SS-2500 (from #2 to #7 as indicated). The scale of all the images is the same as that in (*a*).

temperature is primarily controlled by the nature of the material (i.e. SS or W) in contact with the LM, and that T_w significantly decreased for the flatter #SS substrates. Changes in wetting contact angle of LM have been found on laser patterned SS [8, 9, 33] or as a function of chemical composition of the substrates [34]. Meanwhile, according to figure 5(*b*), T_s values for the #SS substrates were also lower (i.e. below 370 °C) than for the W/#SS specimens, where this parameter increased to ca. 430 °C for the rougher specimens W/#2-500, W/#2-2500 and W/#3-2500 (see table 1 and figure 2).

Photographs in figure 6 characterize the LM spreading capacity of the different specimens. These images along with the measured spreading distances also included in the figure show that the length of LM spreading on the #SS substrates, and specimen W/#SS-500, W/#3-2500 and W/#4-2500 was smaller than that found for W/#2-2500, W#5-2500 and

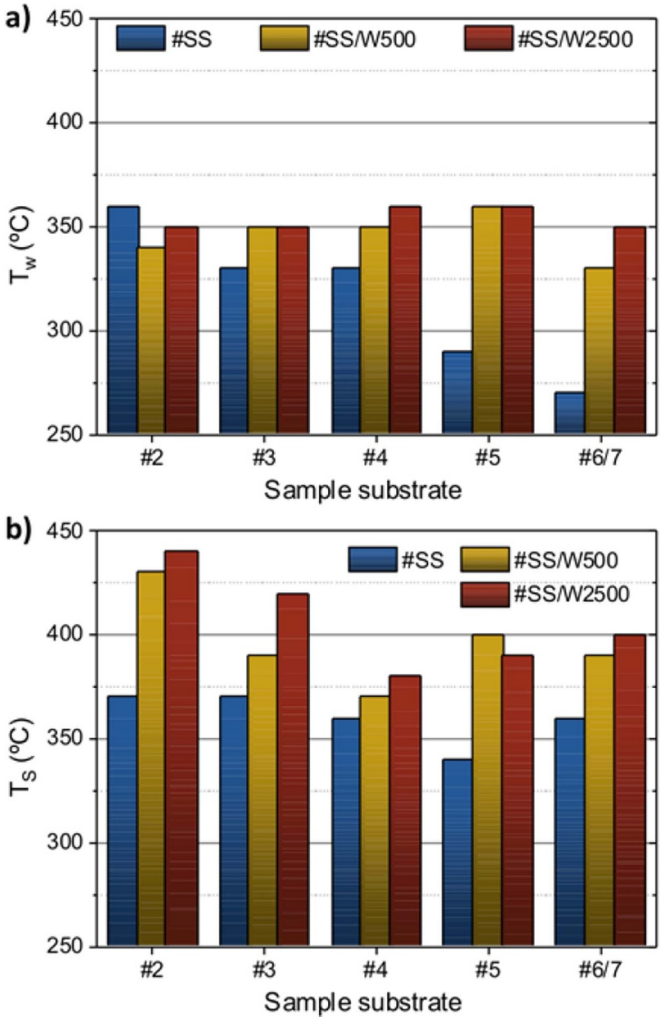

Figure 5. Wetting and spreading temperatures for samples #SS and W/#SS. (*a*) T_w values presented in bar diagrams for W/#SS-500 and W/#SS-2500 specimens prepared onto substrates #2–#6/7 as indicated. (*b*) Idem for T_s values.

W/#6/7-2500, where the front lines reached maximum distances. According to figure 4, a common morphological feature in these four specimens is that deposited tungsten forms well-defined nanocolumns separated by average distances in the order of 1–2 microns and morphological characteristics similar to those reported for sample W/#1-2500 in figure 3. We hypothesize that, similarly than for laser treated surfaces [8, 9], the separation between tungsten nanocolumns and their particular morphology optimize the capillary forces that favor LM spreading through the surface. To get a deeper insight into possible correlations between surface nanostructure and spreading behavior, table 2 summarizes the morphological features of the tungsten layers in the studied *W/#SS-2500* specimen and relates them with the LM spreading capacity. For a more straightforward analysis, the heads of tungsten columns or layers in the micrographs included in this table have been highlighted in yellow using the procedure described in the experimental section.

According to the data in figure 6 and the analysis in table 2, improvement of LM spreading with respect to the bare #SS substrates and specimen W/#SS-500 occurred on specimens W/#2-2500, W/#6-2500 and W/#7-2500, where W forms nanocolumns separated by distances of 1–2 microns, similar to those existing in sample W/#1-2500 (see figure 3). These evidences support that a surface void morphology formed by interconnected channels of this width separating tungsten nanocolumns of a similar height constitutes an optimum topography for the spreading of LM, whereas the existence of wider channels seems to affect very weakly. In this regard, it is interesting that specimens W/#4-2500 and W/#5-2500 depicted a certain anisotropic spreading behavior characterized by a slightly higher LM front line in the direction of the grooves and less in the opposite direction where, according to the analysis in table 2, the tungsten nanocolumns are separated by larger distances (see supplementary material, figure S2). This slight difference sustains that spreading is partially hindered when the distance between W nanocolumns is large, as it happens for the rows of W nanocolumns preferentially grown on the hillocks of grooves existing in these samples. Recent Molecular Dynamic simulations of the capillary forces intervening during the preferential LM spreading in lineal grooves have shown that diffusion capacity strongly depends on surface feature size [35]. In line with these model calculations, our results here open the way to develop surface structures where moving molten Li preferentially in a giving direction would be possible through a proper tailoring of surface void microstructure.

4. Summary and conclusions

The reported Li wetting results indicate that the type of material, either SS or W, directly in contact with the LM is an important factor controlling the wetting temperature. Interestingly, while roughness contributed to increase T_w in SS, it only plays a secondary role for tungsten-terminated surfaces. In this case, the designed differences in tungsten layer microstructures, at least in the range considered in this study, do not significantly affect T_w, but exhibit a substantial effect on the spreading capacity of melted Li, which would be of importance for refilling purposes in fusion reactor applications. In this line, we have developed a methodology to efficiently control the surface microstructure of tungsten films in order to favor the spreading of lithium. The fabrication method of these layers consists of the magnetron sputtering in an oblique angle configuration. Since for real applications a large variety of substrate materials, roughness and terminations are expected to be available, in the present work we have addressed the way the surface topography of a common material as stainless steel may affect the microstructure of W layers grown using this method. Thus, in order to get a clear view of the interplay between the roughness characteristics of this material substrate and the morphology of the tungsten thin films on top, we have modified the surface of the former with different roughness patterns obtained by rather conventional methods (sand blasting, polishing, electropolishing). Then, on the final W-SS systems, we have identified that the optimal tungsten microstructure for LM spreading consisted of 1–3 micron

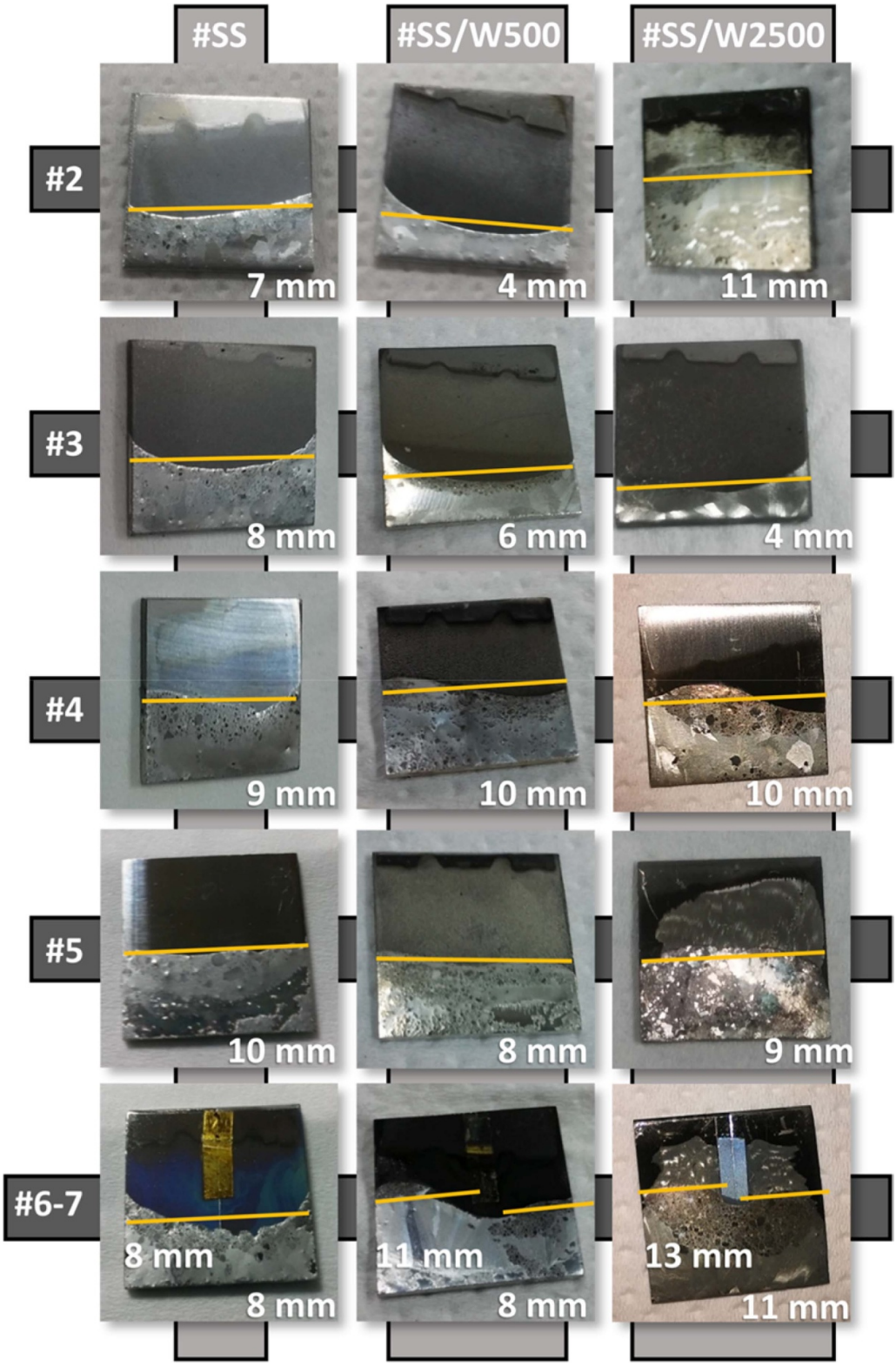

Figure 6. Photographs taken to determine the spreading capacity of LM onto specimens #SS and #SS/W as indicated. Specimens #4/W-2500 and #5/W-2500 in this experiment were oriented with the groove direction perpendicular to the liquid. A line has been drawn signaling the limit of the spreading fronts. The numbers referencing lengths in each image correspond to the spreading distances of the LM from the bottom edge.

Table 2. Morphological features of W structures formed in specimen W/#SS-2500. The size of the images is 16×11 μm.

Sample	Microstructure and tungsten distribution	Description of the morphology of W nanocolumns. Effect on LM spreading.
W/#2-2500	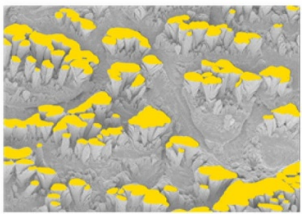	Randomly distributed W nanocolumns formed on the plateaus of SS substrate. *Improvement of LM spreading.*
W/#3-2500	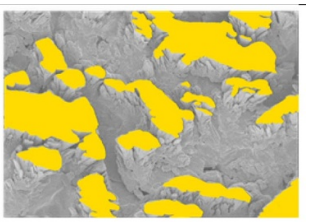	W does not form nanocolumns onto this highly rough substrate. A continuous tungsten layer covers the hillocks of surface features. *No effect on LM spreading*.
W/#4-2500	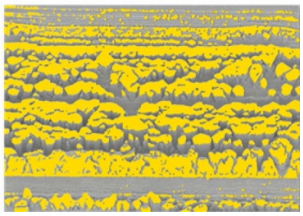	Relatively packed W nanocolumns form on the hillocks of grooves along their direction. These rows of nanocolumns appear separated by the groove width. *No effect on LM spreading*
W/#5-2500	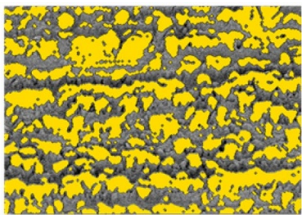	Independent W nanocolumns separated by distances smaller than those found on a flat silicon substrate form preferentially onto the hillocks of grooves. Separation between nanocolumns in the perpendicular direction is equivalent to the groove width. *Little improvement on LM spreading*
W/#6-2500	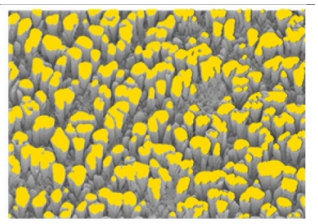	W nanocolumns appear randomly distributed on the SS surface separated with distances similar to those on the flat Si substrate. *Improvement of LM spreading.*
W/#7-2500	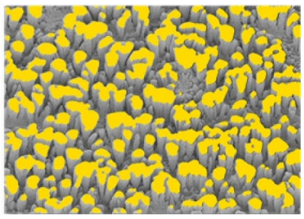	W nanocolumns appear randomly distributed on the SS surface separated with distances similar to those on the Si flat substrate. *Improvement of LM spreading.*

width nanocolumns of tungsten with a height of approximately 2 microns and a separation of approximately 1–2 microns. The analogy of these morphological features with those existing in other CPS systems supports the involvement of surface capillarity effects in the spreading process of the LM. The phenomenology of formation of these nanocolumnar features and its interplay with the roughness characteristics of the substrate have been discussed and justified in the frame of the current models about the growth of oblique angle deposited films onto rough substrates. Finally, some hints have been found suggesting that linearly patterned substrates with a given depth and width of grooves and covered with nanocolumnar tungsten films might be a possible alternative for the anisotropic spreading of LM.

Acknowledgments

This work has been carried out within the framework of the EUROfusion Consortium and has received funding from the

Euratom research and training program 2014-2018 and 2019-2020 under agreement No 633053. Financial support from the EU-FEDER funds, the MINECO (projects MAT2016-79866-R and CSIC 201860E050), Regional Government of Andalusia (project P18-RT-3480) and Madrid (project IND2017/IND-7668), and the University of Seville (V PPIT-US) are also acknowledged. The views and opinions expressed herein do not necessarily reflect those of the European Commission.

ORCID iDs

S. Muñoz-Piña https://orcid.org/0000-0002-8665-9943
A. Garcia-Valenzuela https://orcid.org/0000-0002-5238-6465
J. Gil-Rostra https://orcid.org/0000-0002-4459-4088
V. Rico https://orcid.org/0000-0002-5083-0390
G. Alcalá https://orcid.org/0000-0001-9898-3831
R. Alvarez https://orcid.org/0000-0002-1749-4946
F.L. Tabares https://orcid.org/0000-0001-7045-8672
A. Palmero https://orcid.org/0000-0002-1100-6569
A.R. Gonzalez-Elipe https://orcid.org/0000-0002-6417-1437

References

[1] Wenninger R. *et al* 2017 *Nucl. Fusion* **57** 046002
[2] Lipschultz B. *et al* 2007 *Nucl. Fusion* **47** 1189
[3] Nygren R.E. and Tabarés F.L. 2016 *Nucl. Mater. Energy* **9** 6
[4] Ruzic D.N., Xu W., Andruczyk D. and Jaworski M.A. 2011 *Nucl. Fusion* **51** 102002
[5] Evtikhin V.A., Lyublinski I.E., Vertkov A.V., Belan G., Konkashbaev K. and Nikandrov B. 1999 *J. Nucl. Mater.* **271/272** 396
[6] Tabarés F.L. 2016 *Fusion* **58** 014014
[7] Lin T.F., Palmer T.A., Meinert K.C., Murray N.R. and Majeski R. 2013 *J. Nucl. Mater.* **433** 55
[8] Hammouti S., Holybee B., Christenson M., Szott M., Kalathiparambil K., Stemmley S., Jurczyk B. and Ruzic D.N. 2018 J *Nucl. Mater.* **508** 237
[9] Ruzic D.N. *et al* 2017 *Nucl. Mater. Energy* **12** 1324
[10] Barranco A., Borrás A., González-Elipe A.R. and Palmero A. 2016 *Prog. Mater. Sci.* **76** 59
[11] Hawkeye M.M., Taschuk M.T. and Brett M.J. 2014 *Glancing Angle Deposition of Thin Films: Engineering the Nanoscale* (New York: Wiley)
[12] Alvarez R., Romero-Gómez P., Gil-Rostra J., Cotrino J., Yubero F., Palmero A. and González-Elipe A.R. 2010 *J. Phys. D: Appl. Phys.* **108** 064316
[13] Palmero A., van Hattum E.D., Arnoldbik W.M., Vredenberg A.M. and Habraken F.H.P.M. 2004 *J. Phys. D: Appl. Phys.* **95** 7611
[14] Depla D. and Mahieu S. 2008 *Reactive Sputter Deposition*, (Berlin: Springer)
[15] Toledano D., Escobar Galindo R., Yuste M., Albella J.M. and Sanchez O. 2013 *J. Phys. D: Appl. Phys.* **46** 045306
[16] Garcia-Valenzuela A. *et al* 2019 *Plasma Proc. Polym.* **16** e1800135
[17] Martín M., Salazar P., Alvarez R., Palmero A., López-Santos C., González-Mora J.L. and González-Elipe A.R. 2017 *Sensors Actuators* B **240** 37
[18] Ollitrault J., Martin N., Rauch J.Y., Sanchez J.B. and Berger F. 2015 *Mater. Lett.* **155** 1
[19] Sengstock C., Lopian M., Motemani Y., Borgmann A., Khare C., Buenconsejo P.J.S., Schildhauer T.A., Ludwig A. and Koller M. 2014 *Nanotechnology* **25** 195101
[20] Yoo Y.J., Lim J.H., Lee G.J., Jang K.I. and Song Y.M. 2017 *Nanoscale* **9** 2986
[21] Song C.Y., Larse G.K. and Zhao Y.P. 2013 *Appl. Phys. Lett.* **102** 233101
[22] Godinho V., Moskovkin P., Alvarez R., Caballero-Hernández J., Schierholz R., Bera B., Demarche J., Palmero A., Fernández A. and Lucas S. 2014 *Nanotechnology* **25** 355705
[23] Chen K., Frömter R., Rössler S., Mikuszeit N. and Oepen H.P. 2012 *Phys. Rev.* B **86** 064432
[24] Körner M., Lenz K., Liedke M.O., Strache T., Mücklich A., Keller A., Fracsko S. and Fassbender J. 2009 *Phys. Rev.* B **80** 214401
[25] Liedke M.O. *et al* 2013 *Phys. Rev.* B **87** 024424
[26] Keller A., Peverini L., Grenzer J., Kovacs G.J., Mücklich A. and Facsko S. 2011 *Phys. Rev.* B **84** 035423
[27] Lin C.C. and Hu C.C. 2008 *Electrochim. Acta* **53** 3356
[28] Alvarez R., Garcia-Valenzuela A., Rico V., Garcia-Martin J.M., Cotrino J., Gonzalez-Elipe A.R. and Palmero A. 2019 *Nanotechnology* **30** 475603
[29] Lopez-Santos C., Alvarez R., Garcia-Valenzuela A., Rico V., Loeffer M., Gonzalez-Elipe A.R. and Palmero A. 2016 *Nanotechnology* **27** 395702
[30] Alvarez R. and Palmero A. 2016 Software IDUN for the determination of domains in an image (http://nanoscops.icmse.csic.es/software/idun/)
[31] Pereira A.I., Pérez P., Rodrigues S.C., Mendes A., Madeira L.M. and Tavares C.J. 2015 *Mater. Res. Bull.* **61** 528
[32] Gutiérrez-Delgado A., Domínguez-Cañizares G., Jiménez J.A., Preda I., Díaz-Fernández D., Jiménez-Villacorta F., Castro G.R., Chaboy J. and Soriano L. 2013 *Appl. Surf. Sci.* **276** 832
[33] Wang J. *et al* 2018 *Energy Storage Mater.* **14** 345
[34] Fiflis P., Press A., Xu W., Andruczyk D., Curreli D. and Ruzic D.N. 2014 *Fusion Eng. Des.* **89** 2827
[35] Sun X., Xiao S., Deng H. and Hu W. 2017 *Fusion Eng. Des.* **117** 188